frontiers in Materials

ORIGINAL RESEARCH
published: 11 July 2019
doi: 10.3389/fmats.2019.00154

Monodispersed Hierarchical γ-AlOOH/Fe(OH)$_3$ Micro/Nanoflowers for Efficient Oxygen Evolution Reaction

Wang Huo[1†], Li Li[1†], Yongxing Zhang[1], Jia Li[1], Qianqian Xu[1], Baojie Zhang[1], Lei Zhang[1] and Xuanhua Li[2,3*]*

[1] Department of Materials Science and Engineering, Huaibei Normal University, Huaibei, China, [2] State Key Laboratory of Solidification Processing Center of Nano Energy Materials, School of Materials Science and Engineering, Northwestern Polytechnical University, Xi'an, China, [3] Northwestern Polytechnical University-Queen Mary University of London (NPU-QMUL) Joint Research Institute of Advanced Materials and Structures (JRI-AMAS), Xi'an, China

OPEN ACCESS

Edited by:
Dong Wook Chang,
Pukyong National University,
South Korea

Reviewed by:
Zhao-Qing Liu,
Guangzhou University, China
In-Yup Jeon,
Wonkwang University, South Korea

***Correspondence:**
Yongxing Zhang
zyx07157@mail.ustc.edu.cn
Xuanhua Li
lixh32@nwpu.edu.cn

[†]These authors have contributed equally to this work

Specialty section:
This article was submitted to Energy Materials, a section of the journal Frontiers in Materials

Received: 28 February 2019
Accepted: 17 June 2019
Published: 11 July 2019

Citation:
Huo W, Li L, Zhang Y, Li J, Xu Q, Zhang B, Zhang L and Li X (2019) Monodispersed Hierarchical γ-AlOOH/Fe(OH)$_3$ Micro/Nanoflowers for Efficient Oxygen Evolution Reaction. Front. Mater. 6:154. doi: 10.3389/fmats.2019.00154

Exploring efficient and inexpensive nanostructured catalysts for the oxygen evolution reaction (OER) is critical for economical electrochemical water splitting. Here, monodispersed γ-AlOOH/Fe(OH)$_3$ with hierarchical structures have been synthesized by a facile hydrothermal method and an electrostatic attraction treatment. The low overpotential of only 289 mV at a current density of 10 mA cm^{-2} for γ-AlOOH/Fe(OH)$_3$ with a low Tafel slope of 80.2 mV dec^{-1}, which is greatly decreased than that of γ-AlOOH (347 mV and 88.4 mV dec^{-1}). The monodispersed γ-AlOOH/Fe(OH)$_3$ with hierarchical structures and abundance of surface hydroxyls have high specific surface areas and large pore volumes, which can provide more active sites to help the transfer of the electrons to improve the electrocatalytic performance for OER.

Keywords: hierarchical micro/nanostructures, mesoporous/macroporous structures, electrocatalyst, γ-AlOOH/Fe(OH)$_3$, oxygen evolution reaction, solvothermal method

INTRODUCTION

During the past few years, the electrolysis of water to produce oxygen and hydrogen has become one of the most effective methods to solve the energy crisis and environmental pollution (Sivanantham et al., 2016; Gao et al., 2018; Huang C. et al., 2018; Lan et al., 2018; Nai, 2018; Rajeshkhanna et al., 2018; Wu et al., 2018; Yang et al., 2018a; Zhao et al., 2018; Li X. et al., 2019; Ouyang et al., 2019; Wang J. et al., 2019). However, as an efficiency-determining step for water splitting, the oxygen evolution reaction (OER) is sluggish because it involves multistep four-electron-transfer pathway (Yuan et al., 2014). In the early research, electrocatalytic O_2-productions were dominantly achieved by utilizing precious metal ruthenium (Ru) and iridium (Ir) (Wang et al., 2017). But their high cost and resource scarcity has limited their large-scale practical application. Many efforts have been made to develop novel electrocatalyst with the aim of lower potential and high current density (Anantharaj et al., 2017; Liu D. et al., 2017; Liu G. et al., 2017; Chen and Shi, 2018; Huang Y. et al., 2018; Liu et al., 2018; Li X. et al., 2018; Wang et al., 2018; Xie et al., 2018; Zhang et al., 2018; Wang S. et al., 2019), but substantial progress is still needed to reduce the cost and improve the activity and stability of the OER catalysts.

Metal oxyhydroxide micro/nanomaterials with hierarchical structures, as one of the most promising catalyst, have been widely studied due to their large surface areas, high available active sites and well-defined morphology (Gong et al., 2013; Tang et al., 2014; Yang et al., 2018b; Ye et al., 2018; Li R. et al., 2019). Among them, AlOOH has also been widely studied in photoelectrocatalysis (Roy et al., 2018), photocatalysis (Latifi et al., 2018; Munusamy et al., 2018), antimicrobial activity (Bakina et al., 2018), and determination of toxic metal ions (Qin et al., 2018; Vo et al., 2018) due to its low cost, low toxicity, and environmentally friendly nature. Up to now, there are variable structures of AlOOH, including fiber-like morphologies (Kim et al., 2010), hollow microspheres (Cai et al., 2010; Lan et al., 2013), nanoflakes, and other hierarchical structures, etc. Nevertheless, it still remains urgent to find a way to prepare AlOOH or AlOOH composite electrocatalysts with facile preparation method, high surface area, favorable morphology and excellent electrocatalytic OER properties.

Herein, we prepared an monodispersed γ-AlOOH/Fe(OH)$_3$ composite with hierarchical structures by a facile hydrothermal method and an electrostatic attraction treatment. As far as we know, this is the first report to study the OER electrocatalytic activity of γ-AlOOH/Fe(OH)$_3$ composite. On one hand, the OER performance of as-prepared γ-AlOOH micro/nanoflowers is great due to the favorable morphologies. And on the other hand, with the addition of Fe(OH)$_3$ nanoparticles, there without any change in morphologies, the surface area has been increased and the performance of OER has been improved greatly.

EXPERIMENTAL SECTION

All reagents were of an analytical grade and are commercially available from Sinopharm Chemical Reagent Co., Ltd (China) and were used without further purification.

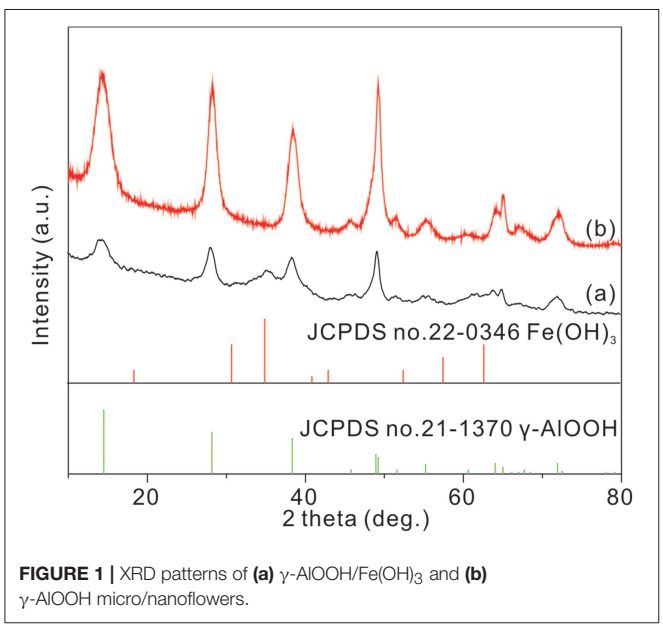

FIGURE 1 | XRD patterns of **(a)** γ-AlOOH/Fe(OH)$_3$ and **(b)** γ-AlOOH micro/nanoflowers.

Synthesis of γ-AlOOH

The hierarchical γ-AlOOH nanomaterials were firstly prepared. In a typical experiment, 1.02 g of sodium aluminate ($NaAlO_2$) and 8.67 g of urea (H_2NCONH_2) was dissolved in 30 mL of deionized water under stirring. And then, 0.20 g polyacrylic acid sodium salt was added into above solution. After being stirred for 30 min, the mixed solution was transferred into a 50 mL Teflon-lined stainless steel autoclave, sealed and maintained at 140°C for 10 h. After the reaction system was naturally cooled to room temperature, the white precipitates was separated from the solution and thoroughly washed three times with deionized water and absolute ethanol, and then dried in a vacuum oven at 60°C for 12 h.

Synthesis of γ-AlOOH/Fe(OH)$_3$ Micro/Nanoflowers

The γ-AlOOH/Fe(OH)$_3$ were synthesized by boiling forcing-hydrolysis method. In a typical synthesis, the monodispersed hierarchical γ-AlOOH (50 mg) were well dispersed in 25 ml deionized water and heated to boiling. Subsequently, 5 ml of the saturated ferric chloride solution was added dropwise to the above boiling solution. Continue to boil the solution until it became reddish brown, turn off the heat. After the reaction system was naturally cooled to room temperature, the precipitate was separated from the solution and thoroughly washed with deionized water and absolute ethanol for several times, and then dried in a vacuum oven at 50°C for 6 h.

Electrochemical Measurements

Five milligram powder of catalyst was dispersed in a mixture of 600 μL water and 400 μl ethanol with 30 μl Nafion solutions, and then the mixture was under continuous ultrasonication for 20 min to obtain a homogenous ink. In a typical experiment, the NF (Ni Foam, about 1 cm*2 cm) was cleaned by 3 M HCl solution for 5 min in an ultrasound bath. And then, the NFs were washed by deionized water and ethanol for 3 times. Then, using a pipette, we extracted the catalyst ink and dropped in the NF. 1 M KOH solution was used as the electrolyte in all the electrochemical process. Pt sheet and Ag/AgCl electrode were employed as the counter and the reference electrodes, respectively. The linear sweep voltammetry (LSV) from 0 to 0.8 V vs. Ag/AgCl with a sweep rate of 1 mV/s. Electrochemical impedance spectroscopy (EIS) were carried out at 0.5 V vs. Ag/AgCl in OER measurement, the frequency scan range was from 1,000 kHz to 0.01 Hz. The pH value of 1 M KOH is ∼14. In this paper, potentials were converted to values referring to the reversible hydrogen electrode (RHE) using the following equation: $E_{RHE} = E_{Ag/AgCl} + 0.197 + 0.059 * pH$, where $E_{Ag/AgCl}$ is the experimentally measured potential against the Ag/AgCl reference electrode. The overpotential (η) was calculated using the formula: $\eta = E_{RHE} - 1.23$.

Characterization

X-ray diffraction (XRD) patterns were obtained in the 2O range of 10–80° using a Philips X'Pert Pro X-ray diffractometer with Cu Kα radiation (1.5418 Å). Field emission scanning electron microscope (FESEM) images were taken on a FESEM (Quanta 200 FEG) operated at an accelerating voltage of 10.0 kV.

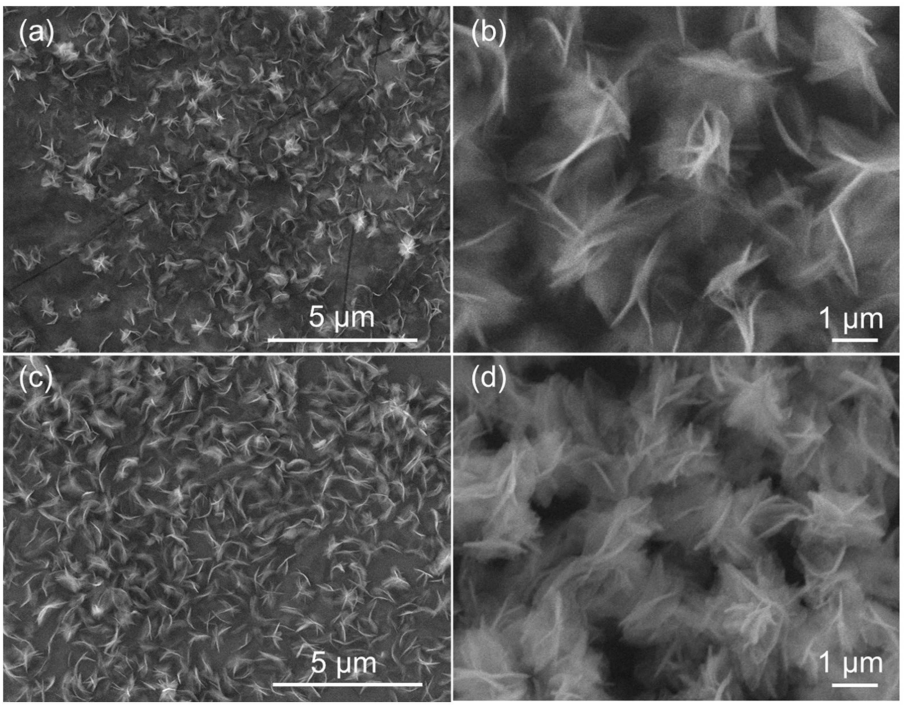

FIGURE 2 | SEM images of the as-prepared **(a,b)** γ-AlOOH, **(c,d)** γ-AlOOH/Fe(OH)$_3$ micro/nanoflowers.

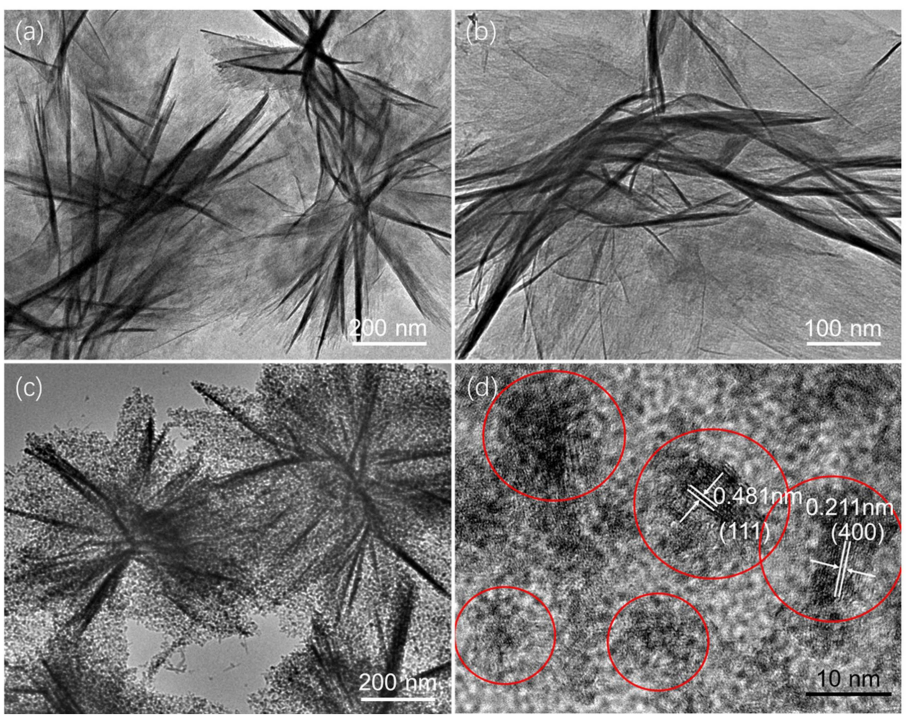

FIGURE 3 | TEM images of the as-prepared **(a,b)** γ-AlOOH, **(c)** γ-AlOOH/Fe(OH)$_3$ micro/nanoflowers, and **(d)** the HRTEM image of Fe(OH)$_3$.

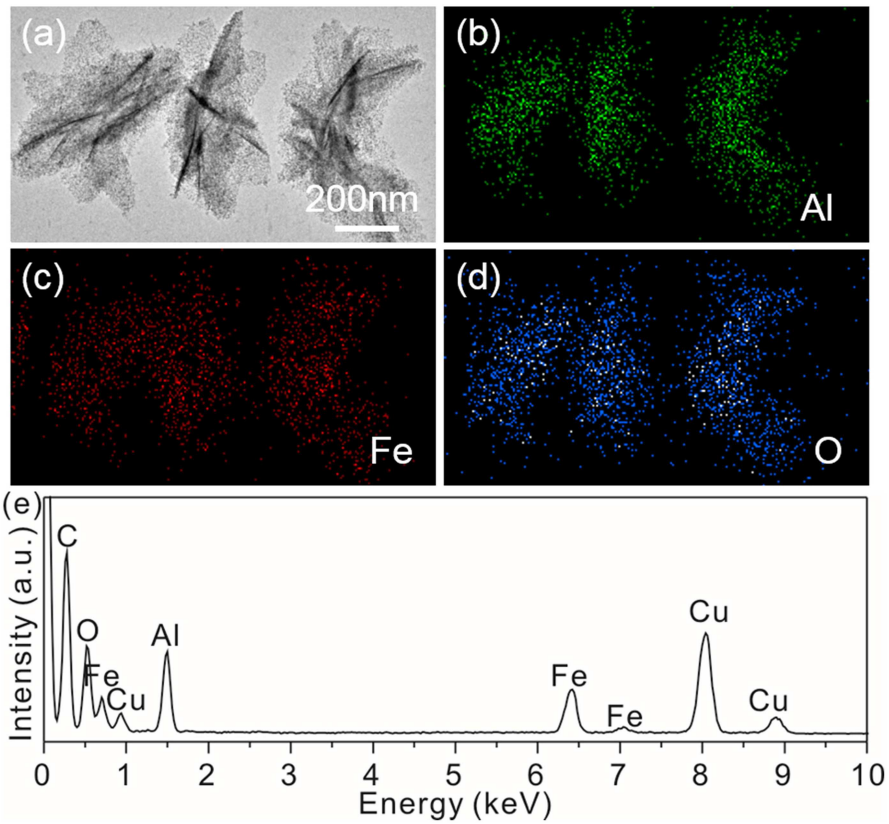

FIGURE 4 | (a) SEM image; Electron energy loss: **(b)** Al, **(c)** Fe and **(d)** O elemental mapping images, **(e)** EDS spectrum of the γ-AlOOH/Fe(OH)$_3$ micro/nanoflowers.

Transmission electron microscope (TEM) images were obtained on a JEOL JEM-2010 high resolution transmission electron microscope, equipped with X-ray energy dispersive spectroscopy (EDS) capabilities, working at an acceleration voltage of 200 kV. The specific surface areas of the samples were measured with Micromeritics ASAP 2020 M$^+$C Brunauer-Emmet-Teller (BET) equipment by using nitrogen adsorption and desorption. The electrochemical measurements were collected by electrochemical system (CHI-760E).

RESULTS AND DISCUSSION

The XRD patterns of the samples are shown in **Figure 1**. From the curve (b) in **Figure 1**, all of the diffraction peaks can be indexed as the γ-AlOOH (JCPDS no. 21-1307). The γ-AlOOH/Fe(OH)$_3$ micro/nanoflowers is confirmed by the XRD pattern in the curve (a) of **Figure 1**. Compared with the curve (b) in **Figure 1**, some additional peaks appear, which can be attributed to the phase of Fe(OH)$_3$ colloid nanoparticles (JCPDS no. 22-0346). This suggests that the sample contains Fe(OH)$_3$ phases. In addition, from the PDF card and the XRD pattern of Fe(OH)$_3$, the obvious peak can be observed at about 35 degrees. The intensity of the XRD pattern of Fe(OH)$_3$ is weak due to the low content of Fe(OH)$_3$.

The morphology and structure of γ-AlOOH and γ-AlOOH/Fe(OH)$_3$ are investigated by SEM as shown in **Figure 2**. From **Figures 2a,b**, there are many monodispersed hierarchical γ-AlOOH micro/nanoflowers with a diameter of 700 nm and the micro/nanoflowers are assembled by nanosheets. The uniform-sized, flower-like and hierarchical structures of the γ-AlOOH/Fe(OH)$_3$ are well-maintained compared to the γ-AlOOH, as shown in **Figures 2c,d**.

The two samples are further investigated by the transmission electron microscopy (TEM) images in **Figure 3**. From **Figures 3a,b**, it is apparent that the structure of γ-AlOOH is assembled by some smooth nanosheets. In addition, there are many particles in the nanosheets in **Figure 3c**, which indicate that Fe(OH)$_3$ colloid particles are successfully adsorbed on the surface of γ-AlOOH nanosheets. And from **Figure 3d**, the diameter of these nanoparticles is about 5 nm (red circles) which may provide more active sites for the OER process. And the lattice stripes with d-spacing of 0.481 and 0.211 nm indexed to (111) and (400) crystal plane of Fe(OH)$_3$ colloid nanoparticles (JCPDS no. 22-0346) can be observed.

In order to further confirm the component and the presence of the Fe(OH)$_3$ on the surface of γ-AlOOH/Fe(OH)$_3$ micro/nanoflowers, they are investigated by electron mapping image analysis (**Figure 4**). Apparently, the different color areas shown in **Figures 4B–D** indicate Al-, Fe-, and O-enriched

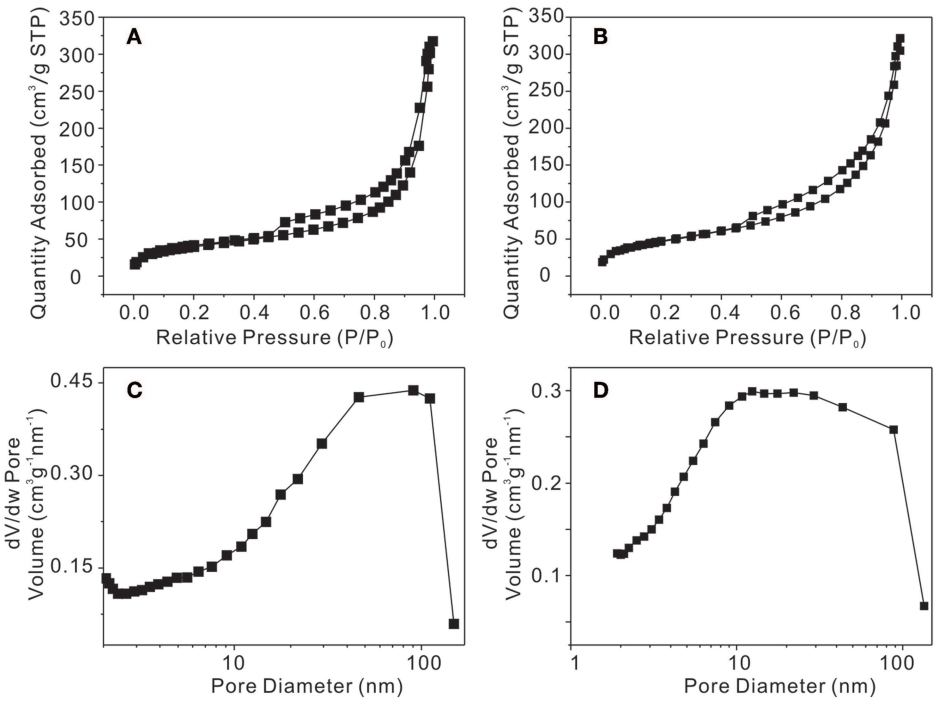

FIGURE 5 | Nitrogen adsorption/desorption isotherm **(A)** γ-AlOOH and **(B)** γ-AlOOH/Fe(OH)$_3$, BJH pore size distribution plot of **(C)** γ-AlOOH and **(D)** γ-AlOOH/Fe(OH)$_3$ micro/nanoflowers.

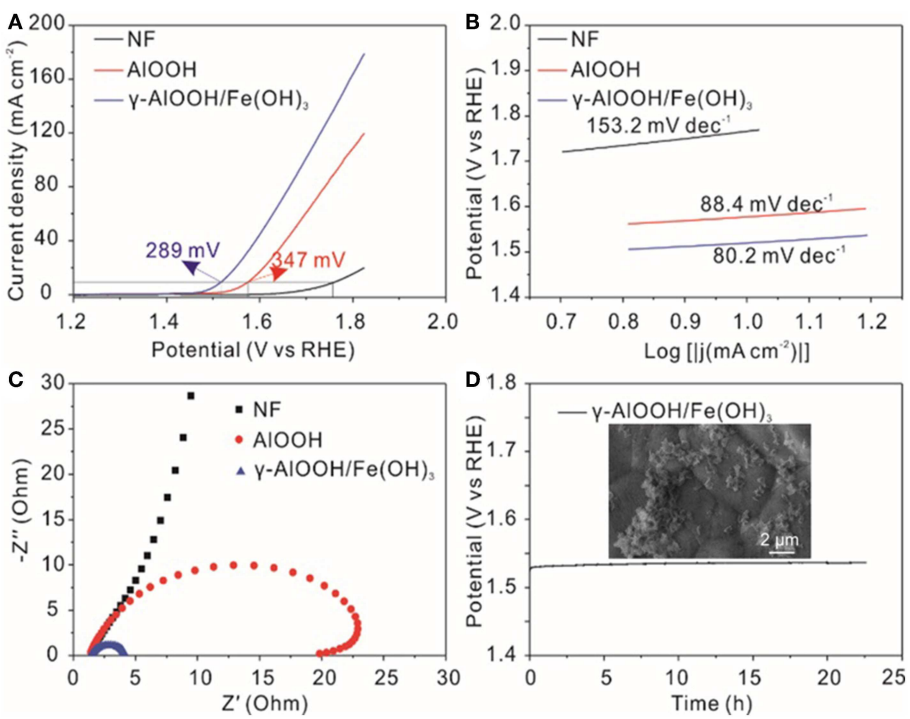

FIGURE 6 | (A) OER polarization curves without iR-compensation, **(B)** Tafel slopes, **(C)** Nyquist plots measured at 0.5 V vs. Ag/AgCl for various catalysts, and **(D)** Durability test at 10 mA cm^{-2} for 22 h of γ-AlOOH/Fe(OH)$_3$ micro/nanoflowers; The SEM image of γ-AlOOH/Fe(OH)$_3$ after i-*t*-test(inset).

TABLE 1 | Summary of OER performances of different electrocatalysts.

Catalysts	η value at 10 mA cm^{-2}	Substrate	References
NF@NC-$CoFe_2O_4$ powders	~300 mV	NF	Lu et al., 2017
NF@NC-$CoFe_2O_4$/C powders	~310 mV	NF	Lu et al., 2017
CoCHH/NF	414 mV	NF	Xie et al., 2017
CoCH/NF	332 mV	NF	Xie et al., 2017
Co_3O_4/NF	~300 mV	NF	Li S. et al., 2018
CoNi/NF	~340 mV	NF	Li S. et al., 2018
Co hydroxide/NF	400 mV	NF	Liu et al., 2018
Fe-Ni hydroxide/NF	325 mV	NF	Liu et al., 2018
$NiCo_2O_4$-R	361 mV	NF	Yang et al., 2018a
$NiCo_2O_4$-N	363 mV	NF	Yang et al., 2018a
Ni_3S_2/NF	300 mV	NF	Sivanantham et al., 2016
$NiCo_2O_4$/NF	330 mV	NF	Sivanantham et al., 2016
γ-AlOOH	347 mV	NF	This work
γ-AlOOH/Fe(OH)$_3$	289 mV	NF	This work

areas of the sample, respectively. The images also show that Al, Fe, and O elements are well-dispersed on the surface of micro/nanoflowers structure. In addition, the EDS data (**Figure 4E**) of the product further reveals the existence of Al, Fe, and O elements. The Cu signal originates from the copper TEM grid.

The N_2 adsorption/desorption isotherm and the pore size distribution of the samples are shown in **Figure 5**. The BET surface area and the total pore volume of γ-AlOOH micro/nanoflowers have been estimated to be 145.523 m^2/g and 0.396 cm^3/g (**Figures 5A,C**), respectively, while γ-AlOOH/Fe(OH)$_3$ micro/nanoflowers is 171.249 m^2/g and 0.400 cm^3/g (**Figures 5B,D**). The BET surface area of γ-AlOOH/Fe(OH)$_3$ micro/nanoflowers is not only higher than that of γ-AlOOH micro/nanoflowers but also higher than the reported values of other γ-AlOOH (Zhang et al., 2006; Feng et al., 2008; Hou et al., 2012; Meng et al., 2014; Abdollahifar et al., 2018). In **Figures 5C,D**, the pore size distribution curve of γ-AlOOH exhibits a broad peak in the range of 2–200 nm with a maximum at 90 nm while γ-AlOOH/Fe(OH)$_3$ is in the range of 2–200 nm with a maximum at 15 nm. The result indicates that there are some mesopores/macropores in the two samples. The change of the maximum value is due to the introduction of the Fe(OH)$_3$ colloid nanoparticles. These mesoporous/macroporous structures and the Fe(OH)$_3$ colloid nanoparticles can be also directly observed from TEM images of the products shown in **Figure 3**.

The electrocatalytic activity of the samples for oxygen evolution reaction (OER) was investigated using a three electrode system in 1.0 M KOH. The linear sweep voltammetry (LSV) of γ-AlOOH, γ-AlOOH/Fe(OH)$_3$ micro/nanoflowers, and pure NF for the OER presented in **Figure 6A** are obtained at a scan rate of 1 mV/s without iR compensation. To judge the efficiencies of the electrocatalyst, there are two pieces of important information that can be collected from these LSV curves, first one is the onset potential and another one is the working over-potential for the generation of 10 mA/cm^2. As it shows, the onset potential of γ-AlOOH/Fe(OH)$_3$ is 1.47 V while γ-AlOOH is 1.52 V, the pure NF is 1.64 V. And the anodic current of γ-AlOOH/Fe(OH)$_3$ increases faster than that of γ-AlOOH, generating the η_{10} of 289 mV, which is lower than that of γ-AlOOH (347 mV) and rivals or outperforms the other catalysts previously reported (see **Table 1**). Actually, the introduction of Fe(OH)$_3$ can increase the number of active surface atoms and provide more active sites to enhance the electrocatalytic activity. To confirm the interior OER kinetics of the as-obtained samples, Tafel slope was directly investigated from the Tafel plot which was generated from the LSV plot. **Figure 6B** depicts the Tafel plots of γ-AlOOH/Fe(OH)$_3$, γ-AlOOH, and pure NF. It is observed that the Tafel slope for γ-AlOOH/Fe(OH)$_3$ is 80.2 mV/dec whereas for γ-AlOOH it is 88.4 mV/dec, demonstrating a faster reaction kinetics. Moreover, electrochemical impedance spectroscopy (EIS) are also conducted to evaluate electron-transfer kinetics in OER of the as-obtained catalysts. As shown in **Figure 6C**, the charge-transfer resistance (R_{ct}) of the γ-AlOOH/Fe(OH)$_3$ is only 1.60 Ω, which is significantly smaller than that of γ-AlOOH (11.2 Ω), revealing that the γ-AlOOH/Fe(OH)$_3$ with the porous hierarchical structure can greatly accelerate the mass transport and electron transfer between the catalyst surface and the reactants. Furthermore, the long-term durability of γ-AlOOH/Fe(OH)$_3$ for OER was assessed by a chronoamperometry measurement for more than 22 h at 10 mA cm^{-2}. In **Figure 6D**, it is found that the potential of the electrode only with negligible increased, manifesting the excellent stability of the γ-AlOOH/Fe(OH)$_3$ toward the OER.

CONCLUSION

In summary, we have successfully obtained monodispersed hierarchical γ-AlOOH micro/nanoflowers in a non-toxic and facile method. And the γ-AlOOH/Fe(OH)$_3$ micro/nanoflowers can be synthesized from the γ-AlOOH precursor without any change on their morphologies by a simply electrostatic attraction treatment. The γ-AlOOH/Fe(OH)$_3$ micro/nanoflowers with high BET surface areas and an abundance of surface hydroxyls which can provide more active sites and speed up the transfer of ions in OER process. Furthermore, this work presents a new method for the preparation of many other oxyhydroxide materials with various morphologies and structures for the oxygen evolution reaction.

DATA AVAILABILITY

The datasets generated for this study are available on request to the corresponding author.

AUTHOR CONTRIBUTIONS

YZ and XL designed experiments. BZ and LZ carried out experiments. JL and QX analyzed experimental results. WH and LL wrote the manuscript.

ACKNOWLEDGMENTS

This research was supported by the Natural Science Foundation of Anhui Province (1708085ME96), the National Natural Science Foundation of China (51571166 and 61505167), the Basic Research Fund for Free Exploration (JCYJ20170815161437298), and the Project of Shaanxi Young Stars in Science and Technology (2017KJXX-18).

REFERENCES

Abdollahifar, M., Hidaryan, M., and Jafari, P. (2018). The role anions on the synthesis of AlOOH nanoparticles using simple solvothermal method. *Bol. Soc. Esp. Ceram.* 57, 66–72. doi: 10.1016/j.bsecv.2017.06.002

Anantharaj, S., Karthik, P. E., and Kundu, S. (2017). Petal-like hierarchical array of ultrathin $Ni(OH)_2$ nanosheets decorated with $Ni(OH)_2$ nanoburls: a highly efficient OER electrocatalyst. *Catal. Sci. Technol.* 7, 882–893. doi: 10.1039/C6CY02282K

Bakina, O. V., Glazkova, E. A., Lozhkomoev, A. S., Lerner, M. I., and Svarovskaya, N. V. (2018). Cellulose acetate fibres surface modified with AlOOH/Cu particles: synthesis, characterization and antimicrobial activity. *Cellulose* 25, 4487–4497. doi: 10.1007/s10570-018-1895-z

Cai, W., Yu, J., Gu, S., and Jaroniec, M. (2010). Facile hydrothermal synthesis of hierarchical boehmite: sulfate-mediated transformation from nanoflakes to hollow microspheres. *Cryst. Growth Des.* 10, 3977–3982. doi: 10.1021/cg100544w

Chen, L., and Shi, J. (2018). Chemical-assisted hydrogen electrocatalytic evolution reaction (CAHER). *J. Mater. Chem. A* 6, 13538–13548. doi: 10.1039/C8TA03741H

Feng, Y., Lu, W., Zhang, L., Bao, X., Yue, B., Lv, Y., et al. (2008). One-step synthesis of hierarchical cantaloupe-like AlOOH superstructures via a hydrothermal route. *Cryst. Growth Des.* 8, 1426–1429. doi: 10.1021/cg7007683

Gao, Q., Shi, Z., Xue, K., Ye, Z., Hong, Z., Yu, X., et al. (2018). Cobalt sulfide aerogel prepared by anion exchange method with enhanced pseudocapacitive and water oxidation performances. *Nanotechnology* 29:215601. doi: 10.1088/1361-6528/aab299

Gong, M., Li, Y., Wang, H., Liang, Y., Wu, J. Z., Zhou, J., et al. (2013). An advanced Ni-Fe layered double hydroxide electrocatalyst for water oxidation. *J. Am. Chem. Soc.* 135, 8452–8455. doi: 10.1021/ja4027715

Hou, H., Zhu, Y., Tang, G., and Hu, Q. (2012). Lamellar γ-AlOOH architectures: synthesis and application for the removal of HCN. *Mater. Characterization* 68, 33–41. doi: 10.1016/j.matchar.2012.03.001

Huang, C., Ouyang, T., Zou, Y., and Li, N. (2018). Ultrathin $NiCo_2P_x$ nanosheets strongly coupled CNTs as efficient and robust electrocatalysts for overall water splitting. *J. Mater. Chem. A* 6, 7420–7427. doi: 10.1039/C7TA11364A

Huang, Y., Chong, X., Liu, C., Liang, Y., and Zhang, B. (2018). Boosting hydrogen production by anodic oxidation of primary amines over a NiSe nanorod electrode. *Angew. Chem. Int. Ed. Engl.* 57, 13163–13166. doi: 10.1002/anie.201807717

Kim, T., Lian, J., Ma, J., Duan, X., and Zheng, W. (2010). Morphology controllable synthesis of γ-Alumina nanostructures via an ionic liquid-assisted hydrothermal route. *Cryst. Growth Des.* 10, 2928–2933. doi: 10.1021/cg901422v

Lan, S., Guo, N., Liu, L., Wu, X., Li, L., and Gan, S. (2013). Facile preparation of hierarchical hollow structure gamma alumina and a study of its adsorption capacity. *Appl. Surf. Sci.* 283, 1032–1040. doi: 10.1016/j.apsusc.2013.07.064

Lan, Y. Q., Wang, X. L., Dong, L. Z., Qiao, M., Tang, Y. J., Liu, J., et al. (2018). Exploring the performance improvement of oxygen evolution reaction in stable bimetal-organic framework system. *Angew. Chem. Int. Ed.* 57, 9660–9664. doi: 10.1002/anie.201803587

Latifi, A. M., Mirzaei, M., Mousavi-Kamazani, M., and Zarghami, Z. (2018). Rice-like Ag/Al_2O_3 nanocomposites preparation from AlOOH nanostructures synthesized via a facile hydrothermal route for azo dyes photocatalytic degradation and Pb^{2+} adsorption. *J. Mater. Sci.* 29, 10234–10245. doi: 10.1007/s10854-018-9074-4

Li, R., Liu, Y., Li, H., Zhang, M., Lu, Y., Zhang, L., et al. (2019). One-step synthesis of NiMn-layered double hydroxide nanosheets efficient for water oxidation. *Small Methods* 3:1800344. doi: 10.1002/smtd.201800344

Li, S., Sirisomboonchai, S., Yoshida, A., An, X., Hao, X., Abudula, A., et al. (2018). Bifunctional $CoNi/CoFe_2O_4$/Ni foam electrodes for efficient overall water splitting at a high current density. *J. Mater. Chem. A*. 6, 19221–19230. doi: 10.1039/C8TA08223E

Li, X., Guo, S., Li, W., Ren, X., Su, J., Song, Q., et al. (2019). Edge-rich MoS2 grown on edge-oriented three-dimensional graphene glass for high-performance hydrogen evolution. *Nano Energy* 57, 388–397. doi: 10.1016/j.nanoen.2018.12.044

Li, X., Wang, X., Xiao, K., and Liu, Z. (2018). *In situ* formation of consubstantial $NiCo_2S_4$ nanorod arrays toward self-standing electrode for high activity supercapacitors and overall water splitting. *J. Power Sources* 402, 116–123. doi: 10.1016/j.jpowsour.2018.09.021

Liu, D., Liu, T., Zhang, L., Qu, F., Du, G., Asiri, A. M., et al. (2017). High-performance urea electrolysis towards less energy-intensive electrochemical hydrogen production using a bifunctional catalyst electrode. *J. Mater. Chem. A* 5, 3208–3213. doi: 10.1039/C6TA11127K

Liu, G., Gao, X., Wang, K., He, D., and Li, J. (2017). Mesoporous nickel-iron binary oxide nanorods for efficient electrocatalytic water oxidation. *Nano Res.* 10, 2096–2105. doi: 10.1007/s12274-016-1398-x

Liu, Q., Zhang, H., Xu, J., Wei, L., Liu, Q., Kong, X. (2018). Facile preparation of amorphous Fe-Co-Ni hydroxide arrays: a highly efficient integrated electrode for water oxidation. *Inorg. Chem.* 57, 15610–15617. doi: 10.1021/acs.inorgchem.8b03063

Lu, X. F., Gu, L. F., Wu, J. X., Liao, P. Q., and Li, G. R. (2017). Bimetal-organic framework derived CoFe2 O4/C porous hybrid nanorod arrays as high-performance electrocatalysts for oxygen evolution reaction. *Adv Mater.* 29:1604437. doi: 10.1002/adma.201604437

Meng, F., Rong, G., Zhang, X., and Huang, W. (2014). Facile hydrothermal synthesis of hierarchically structured γ-AlOOH for fast Congo red removal. *Adv. Mater.* 129, 114–117. doi: 10.1016/j.matlet.2014.05.005

Munusamy, G., Varadharajan, K., Narasimhan, S., and Thangapandiyan, U. G. (2018). Investigation of γ-AlOOH and $NiWO_4$-coated boehmite micro/nanostructure under UV/visible light photocatalysis. *Res. Chem. Intermed.* 44, 7815–7834. doi: 10.1007/s11164-018-3588-5

Nai, J. (2018). Formation of Ti-Fe mixed sulfide nanoboxes for enhanced electrocatalytic oxygen evolution. *J. Mater. Chem. A* 6, 21891–21895. doi: 10.1039/C8TA02334D

Ouyang, T., Ye, Y., Wu, C., Xiao, K., Liu, Z. Q. (2019). Heterostructures comprised of Co/β-Mo_2C-encapsulated N-doped carbon nanotubes as bifunctional electrodes for water splitting. *Angew. Chem. Int. Ed.* 58, 4923–4928. doi: 10.1002/anie.201814262

Qin, D., Hu, X., Dong, Y., Mamat, X., Li, Y., Wågberg, T., et al. (2018). An electrochemical sensor based on green γ-AlOOH-carbonated bacterial cellulose hybrids for simultaneous determination trace levels of Cd(II) and Pb(II) in drinking water. *J. Electrochem. Soc.* 165, B328–B334. doi: 10.1149/2.1321807jes

Rajeshkhanna, G., Kandula, S., Shrestha, K. R., Kim, N. H., and Lee, J. H. (2018). A new class of $Zn_{1-x}Fe_x$-oxyselenide and $Zn_{1-x}Fe_x$-LDH nanostructured material with remarkable bifunctional oxygen and hydrogen evolution electrocatalytic activities for overall water splitting. *Small* 14:e1803638. doi: 10.1002/smll.201803638

Roy, S., Bardhan, S., Pal, K., Ghosh, S., Mandal, P., Das, S., et al. (2018). Crystallinity mediated variation in optical and electrical properties of hydrothermally synthesized boehmite (γ-AlOOH) nanoparticles. *J. Alloy. Compd.* 763, 749–758. doi: 10.1016/j.jallcom.2018.05.356

Sivanantham, A., Ganesan, P., and Shanmugam, S. (2016). Hierarchical $NiCo_2S_4$ nanowire arrays supported on Ni foam: an efficient and durable bifunctional electrocatalyst for oxygen and hydrogen evolution reactions. *Adv. Funct. Mater.* 26, 4661–4672. doi: 10.1002/adfm.201600566

Tang, D., Liu, J., Wu, X., Liu, R., Han, X., Han, Y., et al. (2014). Carbon quantum dot/NiFe layered double-hydroxide composite as a highly efficient electrocatalyst for water oxidation. *ACS Appl. Mater. Inter.* 6, 7918–7925. doi: 10.1021/am501256x

Vo, T. K., Park, H.-K., Nam, C.-W., Kim, S.-D., and Kim, J. (2018). Facile synthesis and characterization of γ-AlOOH/PVA composite granules for Cr(VI) adsorption. *J. Ind. Eng. Chem.* 60, 485–492. doi: 10.1016/j.jiec.2017.11.036

Wang, J., Ouyang, T., Deng, Y., Hong, Y. S., and Liu, Z. Q. (2019). Metallic Mo_2C anchored pyrrolic-N induced N-CNTs/NiS_2 for efficient overall water electrolysis. *J. Power Sources* 420, 108–117. doi: 10.1016/j.jpowsour.2019.02.098

Wang, J., Ouyang, T., Lia, N., Ma, T. (2018). S, N Co-doped carbon nanotube-encapsulated core-shelled CoS_2@Co nanoparticles: efficient and stable bifunctional catalysts for overall water splitting. *Sci. Bull.* 63, 1130–1140. doi: 10.1016/j.scib.2018.07.008

Wang, Q., Shang, L., Shi, R., Zhang, X., Waterhouse, G. I. N., Wu, L. Z., et al. (2017). 3D carbon nanoframe scaffold-immobilized Ni_3FeN nanoparticle electrocatalysts for rechargeable zinc-air batteries' cathodes. *Nano Energy* 40, 382–389. doi: 10.1016/j.nanoen.2017.08.040

Wang, S., Li, Z., Zhang, Y., Liu, X., Han, J., Li, X., et al. (2019). Water-soluble triazolium ionic-liquid-induced surface self-assembly to enhance the stability and efficiency of perovskite solar cells. *Adv. Funct. Mater.* 2019:1900417. doi: 10.1002/adfm.201900417

Wu, R., Xiao, B., Gao, Q., Zheng, Y. R., Zheng, X. S., Zhu, J. F., et al. (2018). A Janus Nickel cobalt phosphide catalyst for high-Efficiency neutral-pH water splitting. *Angew. Chem. Int. Ed. Engl.* 57, 15445–15449. doi: 10.1002/anie.201808929

Xie, J., Qu, H., Lei, F., Peng, X., Liu, W., Gao, L., et al. (2018). Partially amorphous nickel–iron layered double hydroxide nanosheet arrays for robust bifunctional electrocatalysis. *J. Mater. Chem. A* 6, 16121–16129. doi: 10.1039/C8TA05054F

Xie, M., Yang, L., Ji, Y., Wang, Z., Ren, X., Liu, Z., et al. (2017). An amorphous co-carbonate-hydroxide nanowire array for efficient and durable oxygen evolution reaction in carbonate electrolyte. *Nanoscale*. 9, 16612–16615. doi: 10.1039/C7NR07269D

Yang, L., Chen, L., Yang, D., Yu, X., Xue, H., and Feng, L. (2018b). NiMn layered double hydroxide nanosheets/$NiCo_2O_4$, nanowires with surface rich high valence state metal oxide as an efficient electrocatalyst for oxygen evolution reaction. *J. Power Sources* 392, 23–32. doi: 10.1016/j.jpowsour.2018.04.090

Yang, L., Zhang, B., Fang, B., and Feng, L. (2018a). A comparative study of $NiCo_2O_4$ catalyst supported on Ni foam and from solution residuals fabricated by a hydrothermal approach for electrochemical oxygen evolution reaction. *Chem. Commun.* 54, 13151–13154. doi: 10.1039/C8CC08251K

Ye, S. H., Shi, Z. X., Feng, J. X., Tong, Y. X., and Li, G. R. (2018). Activating CoOOH porous nanosheet arrays by partial iron substitution for efficient oxygen evolution reaction. *Angew. Chem. Int. Ed. Engl.* 57, 2672–2676. doi: 10.1002/anie.201712549

Yuan, W., Shen, P. K., and Jiang, S. P. (2014). Controllable synthesis of graphene supported MnO_2 nanowires via self-assembly for enhanced water oxidation in both alkaline and neutral solutions. *J. Mater. Chem. A* 2, 123–129. doi: 10.1039/C3TA13531D

Zhang, B., Jiang, K., Wang, H., and Hu, S. (2018). Fluoride-induced dynamic surface self-reconstruction produces unexpectedly efficient oxygen evolution catalyst. *Nano Lett.* 1, 530–7. doi: 10.1021/acs.nanolett.8b04466

Zhang, J., Liu, S., Lin, J., Song, H., Luo, J., Elssfah, E. M., et al. (2006). Self-assembly of flowerlike γ-AlOOH(boehmite) 3D nanoarchitectures. *J. Phys. Chem. B* 110, 14249–14252. doi: 10.1021/jp062105f

Zhao, X., Li, X., Yan, Y., Xing, Y., Lu, S., Zhao, L., et al. (2018). Electrical and structural engineering of cobalt selenide nanosheets by Mn modulation for efficient oxygen evolution. *Appl. Catal. B Environ.* 236, 569–575. doi: 10.1016/j.apcatb.2018.05.054

Conflict of Interest Statement: The authors declare that the research was conducted in the absence of any commercial or financial relationships that could be construed as a potential conflict of interest.